

First-principles conductance of nanoscale junctions from the polarizability of finite systems

Matthieu J. Verstraete,^{1,3,a)} P. Bokes,^{1,2,3} and R. W. Godby^{1,3}

¹*Department of Physics, University of York, Heslington, York YO10 5DD, United Kingdom*

²*Department of Physics, Faculty of Electrical Engineering and Information Technology, Slovak University of Technology, Ilkovičova 3, 812 19 Bratislava, Slovak Republic*

³*European Theoretical Spectroscopical Facility (ETSF), San Sebastian, Gipuzkoa E-20018, Spain*

(Received 12 December 2008; accepted 12 February 2009; published online 31 March 2009)

A method for the calculation of the conductance of nanoscale electrical junctions is extended to *ab initio* electronic structure methods that make use of the periodic supercell technique and applied to realistic models of metallic wires and break junctions of sodium and gold. The method is systematically controllable and convergeable and can be straightforwardly extended to include more complex processes and interactions. Important issues, about the order in which the thermodynamic and static (small field) limits are taken, are clarified, and characterized further through comparisons to model systems. © 2009 American Institute of Physics. [DOI: 10.1063/1.3096912]

I. INTRODUCTION

Nanoscale and molecular electronics is one of the most active topics of research in physics today;^{1–3} it has very important consequences, both for fundamental research and for industrial processes, which will reach their inherent quantum limits in the decades to come. Accurate methods of theoretical as well as experimental characterization are essential, and many open questions remain about the structure, equilibrium, and dynamics of nanometer-sized systems carrying electrical currents. The *ab initio* simulation of materials properties is in a unique position to develop the scope and our understanding of electronics at the nanoscale, providing the only method of systematic analysis of electronic and structural effects, which are never all simultaneously accessible in an experiment. Present simulations of nanoscale transport usually fall into two categories, either employing time-dependent density functional theory (TDDFT)^{4–6} or various flavors of Landauer–Büttiker-type formulas,^{7–9} sometimes using a nonequilibrium Green's function formalism¹⁰ (for a review see Ref. 9). Due to the way they are formulated, using embedding schemes, these techniques often rely on localized functions (atomic^{8,11–14} or Wannier^{15,16} function) to describe the single particle wave functions of the system. This introduces an inherent difficulty in converging calculations, as the basis sets usually cannot be refined systematically. There is still a great deal of uncertainty about the precision of both experiments, e.g., due to fluctuation in experimental conditions of contact and current flow, and theory, where no standard model is yet accepted as being predictive of experiments, apart from simple cases of continuous contact with conductances of at least one quantum of conductance (G_0). The role and importance of electron-electron^{9,17–21} and electron-vibration^{22–24} interactions have been recognized as an important factor in obtaining the correct transport properties even though satisfactory

treatment for a general system at the *ab initio* level is not yet available.

In the following, we present a method to calculate the conductance of a quantum junction, which can be systematically converged and extended to include the effects of different interactions. The formalism has been previously applied to model systems in one-dimensional²⁵ and jellium slabs²⁶ and is here extended to incorporate three-dimensional (3D) realistic *ab initio* electronic structures at the level of local or semilocal TDDFT. Section II describes the method and how it must be adapted to suit the periodic boundary conditions and supercells which are often used in *ab initio* calculations. Preliminary numerical characterization is carried out in Sec. III. Section IV analyzes the convergence properties of the method and applies it to monatomic wires of sodium. In particular, the possibility of obtaining precise calculations of very low conductances is explored for a tunnel junction. Finally, Sec. V examines the contact geometry and bonding effects for bulk gold electrodes.

II. METHODOLOGY

The conductance of a nanojunction characterizes the long-time dynamics of the electronic response of electrons to a driving electric field.²⁶ While formally the long-time limit demands the study of an extended system, for calculation purposes it is possible to consider a finite model for a finite time and the resulting conductance is obtained by extrapolation of the *conductance function*

$$G^{2P} = \lim_{\omega \rightarrow 0^+} \lim_{L \rightarrow \infty} G^{2P}(\omega, L), \quad (1)$$

where G_{2P} is the two-point conductance (see Ref. 26). The order of limits is important here: the one given characterizes transport in an extended system, whereas the reverse would reflect damped oscillations of density in a finite (even though large) system. The underlying finite system can fulfill any boundary conditions and these do not affect the extrapolated

^{a)}Electronic mail: matthieu.jean.verstraete@gmail.com.

results. We take advantage of this fact and use the periodic boundary conditions and a plane-wave basis for the *ab initio* calculations below.

It is presumed in the following that the junction whose conductance we are searching for is centered at 0 in the middle of the cell (which thus extends from $-L/2$ to $+L/2$).

The calculation of the electronic response function at the level of local or semilocal TDDFT, which then leads to the conduction function [Eq. (1)], proceeds in three steps. First we perform a calculation of the occupied ($e_n < 0$) as well as the unoccupied ($e_n > 0$) eigenenergies e_n and eigenstates $\phi_n(\mathbf{r})$ of the system.

Second, we use the eigenvalues and eigenstates to compose the positive imaginary-time Matsubara Green's function

$$\mathcal{G}(\mathbf{r}, \mathbf{r}'; \tau) = \sum_n \phi_n(\mathbf{r}) \phi_n^*(\mathbf{r}') \frac{e^{-e_n \tau}}{e^{\beta e_n} + 1}, \quad (2)$$

where β is the inverse temperature. As \mathcal{G} is antiperiodic in imaginary time (fermionic) there is no need to specify explicitly its behavior for negative imaginary time.

The electronic response to the total electric field is characterized by the polarizability

$$\begin{aligned} P(\mathbf{r}, \mathbf{r}'; \tau) &= -\mathcal{G}(\mathbf{r}, \mathbf{r}'; \tau) \mathcal{G}(\mathbf{r}', \mathbf{r}; -\tau) \\ &= \mathcal{G}(\mathbf{r}, \mathbf{r}'; \tau) \mathcal{G}(\mathbf{r}', \mathbf{r}; \beta - \tau), \end{aligned} \quad (3)$$

which, after Fourier transformation, $\tau \rightarrow \omega$, and integration over the cross-sectional area of the junction A gives the integrated polarizability relevant for charge transport

$$P(x, x'; i\omega) = \frac{1}{A^2} \int \int dS_{\perp} dS'_{\perp} P(\mathbf{r}, \mathbf{r}'; i\omega). \quad (4)$$

Methods going beyond the present level of approximations, i.e., using nonlocal exchange-correlation kernels^{27,28} or Green-function-based many-body methods,²⁹ would differ in the above Eqs. (2) and (3). The expression for the irreducible polarizability, Eq. (3), would contain further vertex diagrams²⁹ and, in the case of many-body methods, the Green's function cannot be expressed in terms of one-electron wave functions as in Eq. (2). However, the discussion that follows would apply also to these computationally more demanding approaches.

Finally, the third step consists of integrating the polarizability to obtain the conductance function. For an infinitely long system, the conductance is obtained from the expression²⁶

$$G^{2P}(\omega, \infty) = \omega \int_{-\infty}^0 \int_0^{\infty} P(x, x'; i\omega) dx dx', \quad (5)$$

where this integral converges for any finite ω since $P(x, x'; i\omega) \rightarrow 0$ for $x, x' \rightarrow \infty$. The integration region corresponds to choosing the elements of polarizability which connect points on opposite sides of the junction. This is intuitive, as we are interested in how a perturbation on one side can influence charges on the other side, through the junction.

For a finite system of length L we obtain the corresponding function

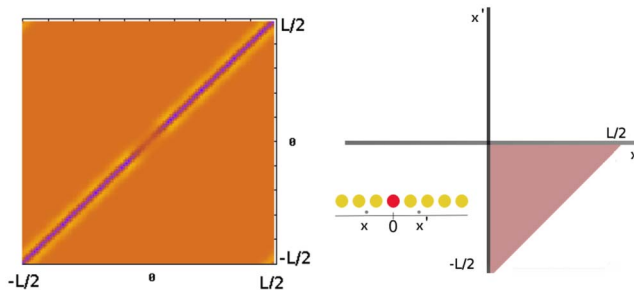


FIG. 1. (Color online) Left: example of a color plot of the polarizability $P(x, x')$ for a junction. P is nonzero only near the diagonal $x=x'$ and lower in the central tunneling region (see below). Right: the region of spatial integration for the polarizability as in Eq. (6). For periodic systems the polarizability will have spurious images, which must be excluded from the integration region. Taking the thermodynamic limit will increase the size L of the system and the triangular domain converges uniformly to the quarter plane $0 < x < \infty$ and $-\infty < x' < 0$. The inset is a cartoon of an atomic wire with a central site and two positions x and x' .

$$G^{2P}(\omega, L) = \omega \int_{\mathcal{D}} P(x, x'; i\omega) dx dx', \quad (6)$$

where \mathcal{D} is a domain of positive x' and negative x which must guarantee the correct limiting procedure. Using a periodic supercell, for $x' - x \rightarrow \pm L$, we approach a periodic image of the system we want to study. Further, if the system is not translationally invariant we will approach a region of the (x, x') plane (the lower right hand corner of Fig. 1), where the polarizability behaves very differently from that near $(0, 0)$ (typically one with a more metallic behavior and larger polarizability than the junction). Hence, a correct integration needs to truncate the quadrant defined by $-L/2 < x < 0$ and $0 < x' < L/2$. For a finite system there is no unique choice of \mathcal{D} , but there is a natural one, which is $0 < x' < L/2$ and $-|x'| < x < 0$, or equivalently $0 < x' - x < L/2$, defining a triangle between 0 and the points $(0, L/2)$ and $(-L/2, 0)$ (Fig. 1).

The finite size of the system determines the minimal frequency which can be reliably described in the conductance, or equivalently the longest time propagation. For longer times or lower frequencies the electrons will reach the limits of the system, and the conductance decays. The minimum frequency may be estimated as

$$\omega_{\min} = 2\pi v_F / L, \quad (7)$$

where v_F is the Fermi speed. Thus, an electron at the Fermi level takes time $1/\omega_{\min}$ to traverse the whole system. This frequency will be essential in determining how to extrapolate the conductance function to zero frequency: Eq. (7) is a rough (in the sense that it comes from a crude approximation for the finite size effects) lower bound for the validity of the conductance function. ω_{\min} always corresponds to a sharp downturn in $G(i\omega)$. In order to calculate the static conductance, one has to extrapolate the conductance curve from an interval in frequency above ω_{\min} down to 0. We will usually extrapolate linearly after finding that the apparent functional form of $G(i\omega)$ changes substantially in the different cases below and is quite different from the analytical jellium result.²⁵ In the following, we will place a dot on conductance

curves at the frequency ω_{\min} and explain the fitting intervals used for the extrapolation of $G(i\omega)$.

We apply the formalism described above to systems described by modern electronic structure methods. Many of these techniques use periodic boundary conditions to describe crystalline structures and represent wave functions and electronic densities using plane wave basis sets. Here we describe the corresponding small changes needed in the formalism.

First, as we wish to describe an isolated nanojunction between two leads (which are in principle infinite) we will use only the zone-center Γ k -point of the Brillouin zone (BZ) along the axis of conduction. Using several k -points would in effect simulate an array of interfering junctions. The periodic boundary conditions are nevertheless exploited as the regions near the edge of the simulation cell are described continuously instead of being brutally cut off or terminated with hydrogen atoms. The thermodynamic limit along the conduction axis must still be ensured by increasing the longitudinal system size until the conductance converges.

In the directions perpendicular to x a denser k -point grid can be used if bulk 3D leads are considered: the electronic structure of the leads will thus be represented correctly, but care must be taken that the transverse distance between images of the “junction” part of the cell is sufficient to avoid interference between periodic images. In the case of a purely 1D system no perpendicular k -points are necessary as the system is supposed to be isolated in vacuum along y and z .

III. NUMERICAL CHARACTERIZATION

In order to understand the convergence behavior of the main results we have also analyzed a finite 1D jellium model and a finite 1D tight-binding (TB) model. The length L of both systems can be made much larger than in the *ab initio* models, which allows a detailed study of the extrapolation to small frequencies. Similar to the *ab initio* case, both models use periodic boundary conditions and their parameters are such that the density and the Fermi speed of the particles will be identical to that of a sodium chain studied within the self-consistent *ab initio* calculations. In fact, the jellium model with a bare electron mass is an excellent model for the sodium wires. This is shown in Fig. 2 where the dispersion of eigenenergies obtained from *ab initio* calculations is compared with the dispersion of the 1D jellium and the fitted TB model. More generally, these two models represent two extremal types of electronic structure for metallic wires. The correct understanding of the extrapolations to infinite size and zero frequency of their conductance functions is very useful for performing extrapolations of more realistic but numerically more demanding *ab initio* calculations.

For both model systems one can find the eigenstates exactly by going into reciprocal space. The conductance function [Eq. (6)] can be expressed using the exact eigenstates of the Hamiltonian

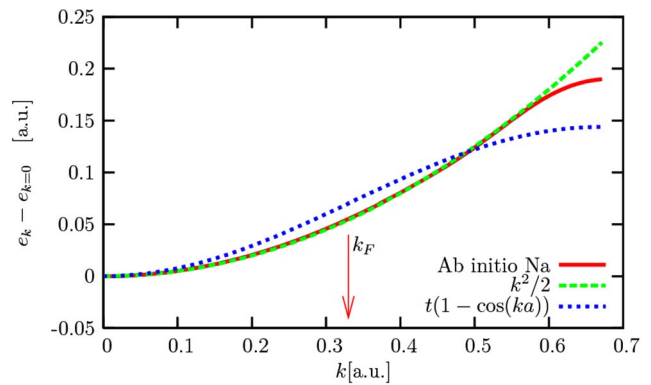


FIG. 2. (Color online) The dispersion of eigenenergies obtained from the *ab initio* calculations (see Sec. IV for details) is almost identical to that of 1D jellium using the bare electron mass. The TB model is fit to have the same Fermi speed, and the differences with respect to the *ab initio* dispersion are more significant.

$$G^{2P}(\omega, L) = 2\omega \sum_{ij} |s(p_i - q_j)|^2 (1 - n_{q_j}) n_{p_i} \times \frac{e^{\beta(e_{p_i} - e_{q_j})} - 1}{i\omega + e_{q_j} - e_{p_i}}, \quad (8)$$

where the sum goes over all eigenstates, p_i or q_j are the momenta of the eigenstates, n_{p_i} are Fermi occupancies of the state p_i at temperature $T = 1/k_B\beta$, e_{p_i} are the eigenenergies corresponding to an eigenstate with the momentum p_i , and the factor 2 accounts for the spin degeneracy. The function $s()$ represents the conductance vertex factor (similar to the expression for conductivity in terms of the polarization function, see, e.g., Bruus and Flensberg³⁰) and takes different forms for the two systems as given below.

The jellium model consists of a 1D noninteracting electron gas of total length L and density $n = N/L$, where N is the total number of electrons. If E_F is the Fermi energy, the eigenvalues are

$$e_{p_i} = \frac{p_i^2}{2} - E_F, \quad p_i = \frac{2\pi}{L}i, i = \pm 1, \pm 2, \dots \quad (9)$$

and the conductance vertex factor is

$$s(p) = \frac{1}{\sqrt{2L}} \int_0^{L/2} dx e^{-ipx} = -\frac{i}{\sqrt{2L}p} (1 - e^{-ipL/2}). \quad (10)$$

The Fermi energy is obtained from the requirement that the charge per unit length is identical to that of the sodium wires; the length L is set to Nd_{Na} , where d_{Na} is the interatomic distance of the sodium wire so that the density of electrons is $n = N/L = 1/d_{\text{Na}}$.

In the case of the tight-binding model, the Hamiltonian has the form

$$H^{\text{TB}} = \sum_{n=-N/2}^{N/2-1} -\frac{t}{2} (c_n^\dagger c_{n-1} + H.c.), \quad (11)$$

with the resulting eigenvalues $e_{p_i} = -t \cos(p_i)$ for a state with momentum p_i . The momentum only takes discrete values

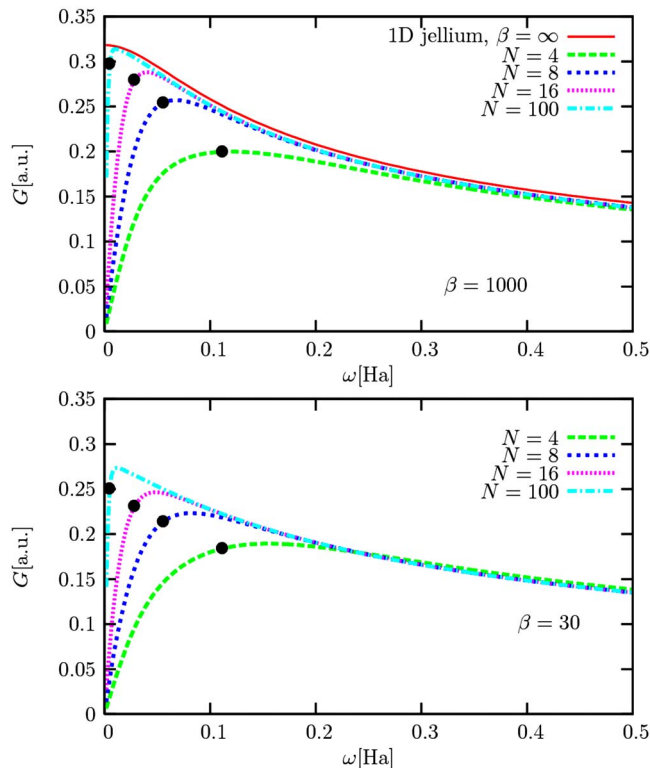


FIG. 3. (Color online) Convergence of the conductance of a jellium wire with respect to system size. The lengths correspond to sodium wires 4, 8, 16, and 100 atoms long. Upper graph: $T \ll E_F$ ($\beta=1000$). Lower graph: $T \sim E_F$ ($\beta=30$). The curves at low temperature approach the analytical infinite-size result (for $T=0$, continuous line). The curves should be extrapolated to zero frequency, disregarding values for $\omega \leq \omega_{\min}$ (indicated by a dot on each curve).

$$p_i = \frac{2\pi}{N}i, \quad i = 0, 1, 2, \dots, N-1 \quad (12)$$

and the conductance vertex factor is

$$s(p) = \frac{1}{\sqrt{2N}} \sum_{n=0}^{N/2} e^{ipn} = \frac{1}{\sqrt{2}} \frac{e^{ip(N/2+1)} - 1}{e^{ip} - 1}. \quad (13)$$

At half filling, the Fermi momentum $k_F = p_{(N/4)}$ and the Fermi speed are $v_F = de(p)/dp = t$. Making use of the Fermi speed of the sodium wires considered in Sec. IV, $v_F = 0.33$ a.u., we identify the TB parameter as $t = v_F/d_{\text{Na}} \approx 0.07$.

The evaluation of expression (8) for both models is very fast and can be done for much longer wires than in the case of first-principles calculations. In the top panel of Fig. 3, we show the conductance functions for jellium wires of lengths $L = Nd_{\text{Na}}$ with $N=4, 8, 16$, and 100 at temperatures much lower than the Fermi energy. The curves converge smoothly to the zero-temperature infinite-length limit that is known analytically²⁵ and readily give the static limit of one quantum of conductance $G^{2P}(0, \infty) = 2e^2/h = 1/\pi$ a.u. Furthermore, the functional form shows finite size effects (the downturn of the conductance) according to the expected criterion [Eq. (7)]

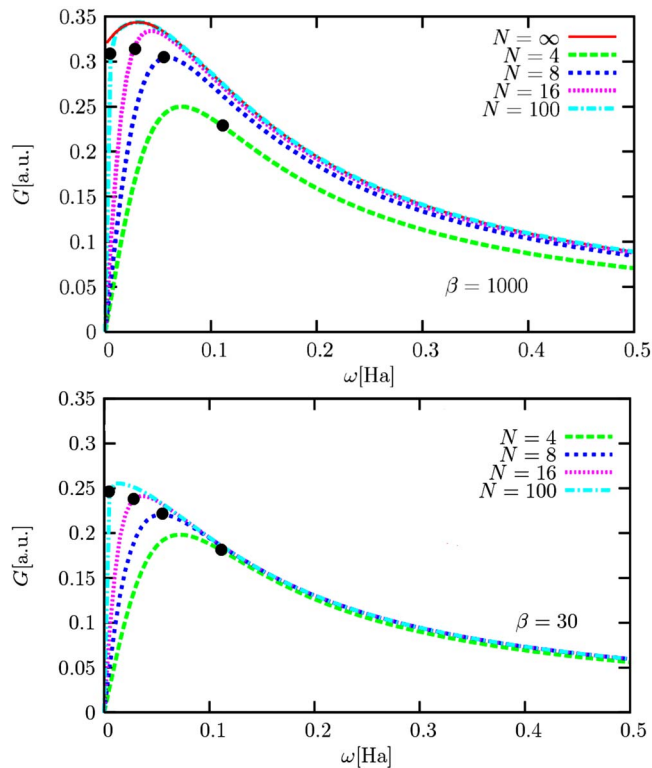


FIG. 4. (Color online) Convergence of the conductance function of a tight-binding model with respect to system size (4, 8, 16, and 100 atoms). v_F is fixed to that of the sodium wire. Upper graph: $T \ll 2t$ ($\beta=1000$). Lower graph: $T \sim 2t$ ($\beta=30$), where $2t$ is the bandwidth. The curves give the correct zero temperature conductance for $L \rightarrow \infty$, but the extrapolation to $\omega=0$ is complicated by the nonmonotonic behavior at small frequencies.

$$\omega_{\min} = \frac{0.44}{N} = 0.11, 0.05, 0.03, 0.004 \quad (14)$$

for $N=4, 8, 16, 100$, respectively. The extrapolation for $N=8$ or $N=16$ gives good estimates of the conductance through the limit in Eq. (6). Note that one should not extrapolate the values of $G(\omega_{\min})$ as the extrapolation of a lower bound will only give a lower bound for the true static conductance (unless the system size is exhaustively converged). Instead, at a given system size, $G(i\omega)$ can be linearly extrapolated to $G(0)$ from the region above the downturn. At temperatures comparable with the Fermi energy (bottom graph in Fig. 3) the extrapolated value is somewhat below the zero temperature limit but the functional form of the conductance is essentially identical.

On the other hand, the tight-binding model, shown in Fig. 4, offers less reliable extrapolations (at low temperatures, upper panel). This is caused by the nonmonotonic behavior of the conductance function at small frequencies, which in turn arises because of the bandwidth of the model (here the bandwidth is $2t=0.14$ a.u.). Thus, if we use the ω_{\min} criterion and trust the conductance function just above, $G(0)$ will be overestimated and will converge quite slowly with system size. In contrast to the jellium case, we do not have the analytical result for an infinite size chain and arbitrary imaginary frequency; instead as the $N=\infty$ curve we use the overconverged results for $N=1000$ and $N=5000$, which are numerically identical in the interval of frequencies shown

in Fig. 4. This demonstrates that the nonmonotonic behavior is not a finite size feature. The behavior weakens if we look at the conductance curve at higher electronic temperature. This is shown in the lower graph in Fig. 4 for a temperature comparable to the bandwidth. For these temperatures the conductance function can be easily extrapolated to (high T) conductance values identical to the jellium model (Fig. 3, lower graph). This suggests that in principle, by performing the calculations at different electronic temperatures or smearing, one may enhance the extrapolation procedure in realistic calculations, which may combine aspects of free-electron (jellium) and localized electron (TB) behaviors. In practice, even in low conductance cases, we have seen no indication of the tight-binding behavior of G in the *ab initio* calculations. The behavior is probably an artifact of the finite TB electronic structure.

To summarize, the models show good convergence in the extrapolated conductance at $\omega=0$ for systems of length equivalent to 8 or 16 atoms. The jellium dispersion is quite close to the *ab initio* ones below, whereas the tight binding one is not—this could be expected from the metallic nature of the junctions. The conductance function of the TB chain is qualitatively different and actually overshoots the quantum of conductance for small imaginary frequencies and large L . Finally, for high temperature (T comparable to E_F) both models depart from the analytic curves for $T=0$ and the conductance decreases.

IV. SODIUM MONOWIRES: SIZE CONVERGENCE AND ENERGY DEPENDENCIES

We begin the *ab initio* studies with a prototypical application: the calculation of the conductance of a uniform monoatomic wire (monowire) of sodium atoms. With one s electron per atom and given the simple-metal nature of sodium, the conductance in the independent particle case will be two quanta of conductance due to spin degeneracy.

A. Technical details

The ground state wave functions and electronic structure are calculated within the density functional theory (DFT)^{31,32} using a plane wave representation with the ABINIT (Ref. 33) or SFHNGX (Ref. 34) codes (the results have been checked to be independent of the ground state code used). We employ norm-conserving Troullier–Martins-type³⁵ pseudopotentials with nonlinear core corrections³⁶ and the d channel as a local potential. The kinetic energy cutoff (20 hartree) and number of bands (100 per Na atom) were overconverged to allow for full checks of the convergence of the conductance calculation. The calculation of the conductance in a module of the GWST code³⁷ was carried out with a kinetic energy cutoff of 8 hartree.

The interatomic distance was set to 2.477 Å. Other distances were checked but did not influence the results appreciably: the Fermi point for the wire is fixed by the parabolic nature of the bands, and, most importantly in our case, the Fermi speed scales as the interatomic spacing, making the critical minimum frequency [Eq. (7)] independent of the spacing.

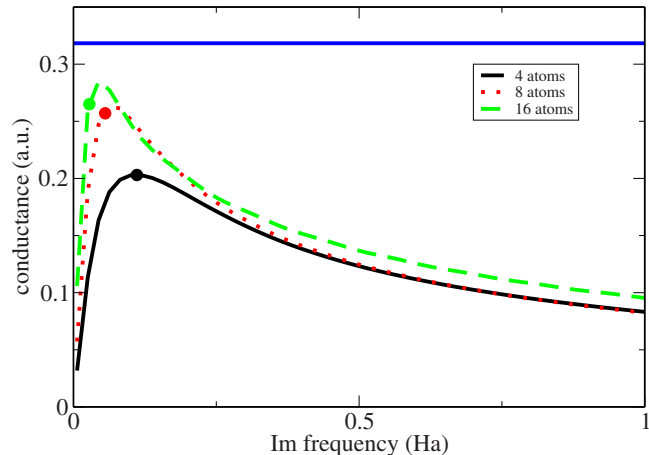


FIG. 5. (Color online) Convergence of the conductance of a continuous monowire of sodium atoms with respect to cell size (4, 8, and 16 atoms in the unit cell). The minimum frequency for which the conductance function is valid depends on the Fermi speed and goes down with increasing system size. For eight atoms the extrapolation to zero frequency is already good, arriving close to the expected two quanta of conductance (horizontal line) for a noninteracting system with spin degeneracy.

The perpendicular size of the unit cell is more important, as we wish to simulate a truly 1D system using a supercell. The lateral dimensions of the unit cell are fixed to 4 Å, which is enough to ensure that conductance only happens along the wire direction. Checks with 8 and 16 Å cells showed that the conductance function is already well reproduced to within a few percent.

B. Results for uniform Na monowires

Figure 5 shows the size convergence of the conductance function for unit cells containing 4, 8, and 16 atoms. As can be seen in this simple case the conductance function is correct to lower and lower frequencies as the system size is increased, and the extrapolation tends toward $1/\pi$. Already with an eight atom cell the linear extrapolation of G^{2P} to zero frequency gives a value very close to $1/\pi$, as expected from section III. Comparing the values obtained for successively larger system sizes gives an estimate of the residual error in converging L . A 16 atom unit cell is about 40 Å long. The very slow convergence of $G(\omega_{\min}, L)$ as a function of L is due to the 1D character of the system. Coulomb screening in one dimension is quite inefficient and the polarizability decays quite slowly. In 3D systems the screening will be stronger and the size convergence quicker.

A very important point is to have a good estimate of the Fermi level. In 1D atomic chains this is not trivial, as the equivalent of k -point sampling is the length of the system. The distance between the levels bracketing the E_F decreases with L , but not uniformly. For small L , there is an alternation in the position of the Fermi level: for wire lengths which are multiples of 4 the Fermi level is exactly on a single particle state, whereas for other values it is higher and between states. The dielectric response of these two cases is very different, as one case appears to be a metal and the other an insulator (whose gap goes to 0 as $L \rightarrow \infty$). In the interest of brevity we have not included the results for $L=Nd_{\text{Na}}$ with $N=5,6,7$ in Fig. 5: they oscillate slightly (as a function of

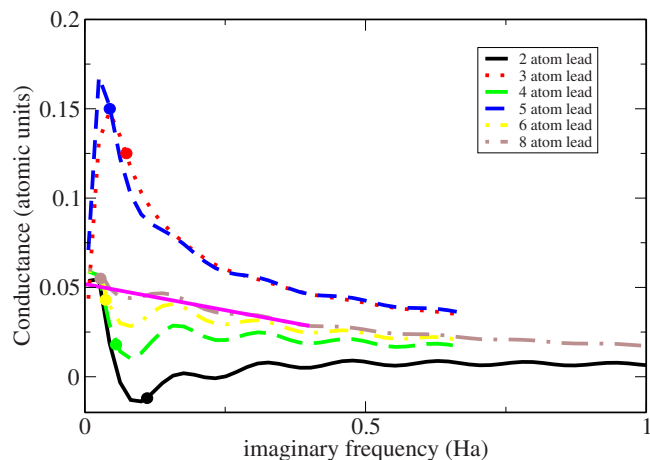


FIG. 6. (Color online) Convergence of the conductance of a wire with a gap (one atom missing) with respect to the size of the lead wires (two to eight atoms in each lead). The conductance functions converge well for even numbers of atoms in the leads due to a correct positioning of the Fermi level and can be extrapolated to zero frequency (the line segment extrapolates from eight-atom lead case). With odd numbers of atoms the Fermi level is positioned in an artificial gap.

N) and converge more slowly, although to the same end result. We will see these effects again in section C for the case of a wire with a gap.

In our formulation the conductance is expressed in imaginary frequency. This implies contributions from all electron hole pairs in the polarizability, not just those for states near the E_F . Because of this the convergence in the number of states is comparable to (but slightly faster than) that of a GW calculation²⁹ with between 5 and 20 bands per electron (for Na wires we need ten bands per electron).

C. Na monowires with a gap

We now proceed with an inhomogeneous case: a wire of Na atoms with a gap (of width d). This is the simplest example of a nanojunction. The conductance will naturally go into a tunneling regime as the gap becomes wider. This example is important because first it has a simple dielectric response and also because tunneling is an important and extreme regime for the conductance. Figure 6 shows the size convergence of a wire with a gap of one atom. The two remaining parts of the wire are of equal length, increasing from two to eight atoms (each). The even length leads converge relatively quickly to a regular conductance function from below. The odd length leads converge from above but very slowly because the highest occupied molecular orbital/lowest unoccupied molecular orbital states are quite far apart, which give a badly placed Fermi level, as above for continuous wires (bad in the sense that it is far from the limiting Fermi level for an infinite system). Extrapolation to 0 frequency gives a conductance of 0.05 a.u. (± 0.005).

The oscillations of $G(\omega)$ are due to aliasing effects in the Fourier transform from imaginary time to imaginary frequency. These are in some cases difficult to eliminate for very low amplitude elements of $P(x, x', i\tau)$.

Finally we consider the transition from the conducting to the tunneling regime by increasing the gap size (for eight atom leads). The conductance functions are represented in

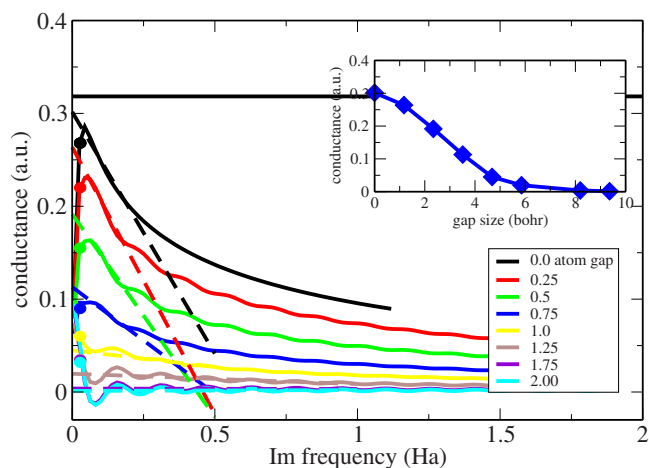


FIG. 7. (Color online) Conductance function of gapped wires with respect to imaginary frequency and for different gap sizes (in fractions of the interatomic distance in the regular wire). There are eight atoms in each lead. Inset: extrapolated 0 frequency conductance as a function of gap length. The conductance saturates for small gaps, and for gaps larger than ~ 0.75 interatomic distances the tunneling decay appears.

Fig. 7 with the inset showing the decrease in the extrapolated static conductance as a function of the size of the gap. The conductance decreases with gap size, and by a gap of $3/4$ of an atomic spacing (about 4 bohr) the tunneling regime begins with exponential decay of G . The tail of $G(d)$ gives a very good fit to $G(d) = 1.68 \exp(-0.770d)$, where d and G are in atomic units. The dashed lines are linear extrapolations of G fit to the interval $[0.05, 0.2]$ Hartree. For the lowest curves (largest gaps) the fit was performed further out on $[0.2, 1]$ as the functions are flatter and the aliasing noise more important. In this way we are able to represent quite small conductance values down to 0.001 a.u. (or $0.003G_0$).

A similar system was examined by Beste *et al.*¹⁴ but with gold chains instead of Na. They find a conductance of about 0.12 a.u. for a gap of $d_{Au}/2$ (1.28 Å), which is close to our value of 0.18 a.u. for $d_{Na}/2$. One important conclusion of Ref. 14 is the very strong deviations that can appear depending on the basis set nature with localized basis sets. Our results can be converged systematically using a plane-wave basis set, but probably heavier calculations as a trade off.

V. GOLD WIRES: LEAD STRUCTURE AND K-POINT SAMPLING

We now proceed to a more structured system showing an explicit constriction. A gold junction is made from a two atom wire contacted to bulk 3D electrodes. The electrodes are fcc stacked gold (at the experimental nearest neighbor distance of 2.9 Å in Ref. 38) of which we use a 2×2 (111) surface unit cell. The wire atoms are evenly spaced with the fcc interlayer distance of 2.37 Å (which is compressed compared to the DFT-local-density approximation (LDA) equilibrium distance of 2.5 Å for the infinite straight wire³⁹). No relaxation of atomic positions with respect to the bulk is taken into account, but the addition of further structural effects is in no way more difficult; contrary to some other approaches to transport^{4,14} we are not constrained to specific unit cell lengths or layer spacings. A typical unit cell is

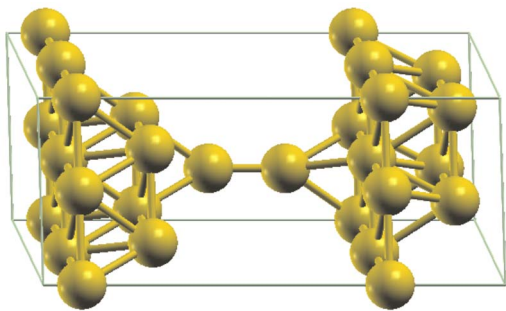


FIG. 8. (Color online) Unit cell of a short gold wire contacted with bulk gold electrodes, which are two layers thick. Both atoms sit at natural fcc hollow positions on the (111) surfaces.

shown in Fig. 8 for the minimal electrode thickness of two layers (in each electrode). Electrodes 3 and 4 layers thick were also tested. Because of periodicity and in order to maintain a continuous fcc structure at the cell boundary, the point of contact of the wire to the right electrode alternates between the different possible fcc stacking sites (for two and four layer electrodes) and an on-top position (for three layer electrodes). We find a little effect of contact position on the conductance of the junction (see below) in this continuously metallic, well contacted case.

A. Technical details

The pseudopotential we use is of the Hartwigsen–Goedecker–Hutter (HGH) flavor⁴⁰ with only the 6s electrons in the valence. Our choice of pseudopotential is justified by its softness, by the chemical homogeneity of the system, and our intention to go beyond LDA and include many-body corrections. We have performed tests on fcc gold in the GW approximation (which is beyond the scope of the present article), including the 5d electrons. The problems recognized by Marini *et al.*⁴¹ for Cu appear for Au as well: the exchange self-energy is quite badly represented for the 5d electron states due to the absence of the 5s and 5p. The latter are far in energy but have an important spatial overlap with the 5d. Consequently, the exchange self-energy lacks important contributions if one uses only the valence electrons. The GW *d* bands are very poor (whereas their position in LDA is very close to experimental values); some bands are pushed down and others up to the Fermi level, which would change the conductance severely. The use of a purely 6s potential is less realistic but reduces these exchange effects (which are now between the 6s and the core 5d states). A more complete solution is that adopted by Shishkin and Kresse⁴² in the PAW formalism.⁴³ As PAW allows explicit reconstruction of the core states, the exchange with the valence can be calculated explicitly. Finally, the *d* electrons do not complexify the independent particle conductance calculation formally, but do make the calculations much heavier (with additional ten electrons per atom). As the states at the Fermi level are purely *s*-electronlike, the conductance will not be affected strongly. However, as our method is an integral of the dielectric response of the system, the absence of the *d* electrons will have an indirect effect through changes in the polarizability.

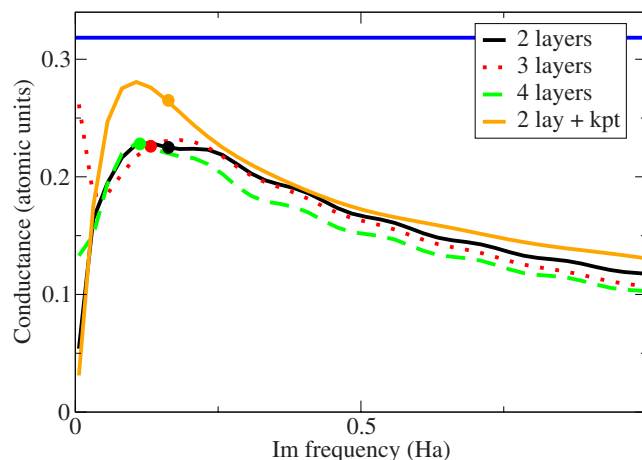


FIG. 9. (Color online) Conductance functions of gold junctions containing a two atom wire and bulk fcc leads. For 2, 3, and 4 layers of gold in the leads and only the Γ *k*-point (solid black, dotted, and dashed) and for two layers of gold and a 4×4 sampling of the BZ perpendicular to the wire axis (solid orange curve). The horizontal line is the quantum of conductance. The peak in the conductance moves to lower energies as the system length is increased. In the case with denser BZ sampling the conductance function is much better represented even if the minimum frequency has not changed.

B. Results

From a calculation of a uniform wire (with *k*-points along the wire axis), we estimate the Fermi speed in the wire to be 0.42 a.u. (1.9×10^6 m/s), corresponding to a wavelength of 7.22 bohr. A simple metal approximation for the bulk gives an estimated Fermi speed of 0.64 a.u. (1.4×10^6 m/s) from the Au Seitz radius. A DFT calculation of fcc bulk naturally gives a more complex band structure—the modulus of the Fermi speed varies by some 20% in reciprocal space. The HGH pseudopotential gives an average value of 1.02 a.u. (2.2×10^6 m/s). A more complete pseudopotential with *d* electrons reduces this value to 0.67 a.u. (1.5×10^6 m/s). The value we are interested in is the speed of propagation of an electronic signal through the whole system, i.e., through the 3D bulk (with the pseudopotential we are using) and the wire, which will be between the pure bulk and pure wire values. With the bulk and wire v_F , we can estimate the minimal frequencies that can be represented for different unit cell sizes. With cells of lengths 27, 36, and 45 bohr, we obtain $\omega_{\min} = 0.163, 0.132, \text{ and } 0.113$ hartree.

In Fig. 9 (lowest three curves) we represent the conductance as a function of imaginary frequency for a series of gold junctions (like that schematized in Fig. 8) with 2, 3, and 4 layers of fcc gold in the bulk leads. As before for linear wires, initially only the Γ point wave functions are used and $G(\omega)$ takes similar values to the case without leads, which would suggest a similar system length of ~ 8 layers in each lead to converge the conductance. The extrapolated value close to the quantum of conductance is in agreement with the results of the more extended models of the monatomic gold contacts.⁴⁴

With bulk leads it is essential to look at *k*-point convergence: to represent the bulk states correctly, we increase the sampling of *k*-points in the direction perpendicular to the junction axis. Again, as noted above, one must also take care to keep the nanojunctions themselves well isolated in the

perpendicular direction to avoid interference effects, which would be amplified by the perpendicular k -points. With two layer leads and a 4×4 sampling of k -points, we find the conductance function shown by the top curve of Fig. 9. The low frequency behavior is now much closer to that of the longer Na wires. Thus increasing the lead size has two effects, which are controllable separately in this 3D case: first, improving the representation of the density of states (DOS) (which can also be achieved by using the perpendicular k -points if the leads are bulklike), and second, lowering the minimum representable frequency ω_{\min} (which can only be achieved by increasing the system length L). In the future, a more extended study will combine the effects of longer leads and perpendicular k -point sampling, but the computational load will require the parallelization of our code, which is underway.

To summarize, the bulk leads on gold wires show that even with relatively small system sizes a constriction limits the conductance to a single quantum of conductance. Bulk 3D leads give much stronger screening than 1D ones and faster convergence of the conductance function. Including k -points to sample the perpendicular electronic states in the leads improves the description of the DOS and the screening.

VI. CONCLUSIONS

We present a new method to calculate the transport properties of nanoscopic junctions. The extension of the basic formalism to periodic systems and realistic electronic structure is detailed, and the convergence properties are compared to model systems. Order-of-limit problems are reviewed, which also concern many other approaches to quantum transport, as well as numerical issues. The differences and inherent advantages of the method are discussed, in particular the way it treats electrodes and its systematic convergeability in the number of single particle states and the spatial representation of different quantities. Applications to sodium and gold nanojunctions are presented. The first shows the properties of purely 1D systems and demonstrates the variation between regimes of continuous metallicity and of tunnel junctions. The gold junctions explore contact geometries and some of the fundamental differences between 1D and 3D electrode structure and screening.

ACKNOWLEDGMENTS

The authors wish to acknowledge the fruitful discussions with A. Ferretti, P. Rinke, and C. Freysoldt. This research has been supported by the NANOQUANTA EU Network of Excellence (Grant No. NMP4-CT-2004-500198), the NATO Security Through Science Programme (Grant No. EAP.RIG.981521), and by the Marie Curie fellowship (Grant No. MEIF-CT-2005-024152). Some computer time was provided by the White Rose Grid.

¹L. Venkataraman, J. E. Klare, C. Nuckolls, M. S. Hybertsen, and M. L. Steigerwald, *Nature (London)* **442**, 904 (2006).

²S. Y. Quek, L. Venkataraman, Y. J. Choi, S. G. Louie, M. S. Hybertsen,

and J. B. Neaton, *Nano Lett.* **7**, 3477 (2007).

³L. Venema, *Nature (London)* **453**, 996 (2008).

⁴S. Kurth, G. Stefanucci, C.-O. Almbladh, A. Rubio, and E. K. U. Gross, *Phys. Rev. B* **72**, 035308 (2005).

⁵N. Bushong, N. Sai, and M. Di Ventra, *Nano Lett.* **5**, 2569 (2005).

⁶X. Qian, J. Li, X. Lin, and S. Yip, *Phys. Rev. B* **73**, 035408 (2006).

⁷M. Di Ventra, S. T. Pantelides, and N. D. Lang, *Phys. Rev. Lett.* **84**, 979 (2000).

⁸F. Evers, F. Weigend, and M. Koentopp, *Phys. Rev. B* **69**, 235411 (2004).

⁹M. Koentopp, C. Chang, K. Burke, and R. Car, *J. Phys.: Condens. Matter* **20**, 083203 (2008).

¹⁰L. Keldysh, *Sov. Phys. JETP* **20**, 1018 (1965).

¹¹M. Brandbyge, J. L. Mozos, P. Ordejon, J. Taylor, and K. Stokbro, *Phys. Rev. B* **65**, 165401 (2002).

¹²C. Toher, A. Filippetti, S. Sanvito, and K. Burke, *Phys. Rev. Lett.* **95**, 146402 (2005).

¹³H. J. Choi, M. L. Cohen, and S. G. Louie, *Phys. Rev. B* **76**, 155420 (2007).

¹⁴A. Beste, V. Meunier, and R. J. Harrison, *J. Chem. Phys.* **128**, 154713 (2008).

¹⁵A. Calzolari, N. Marzari, I. Souza, and M. Buongiorno Nardelli, *Phys. Rev. B* **69**, 035108 (2004).

¹⁶M. Strange, I. S. Kristensen, K. S. Thygesen, and K. W. Jacobsen, *J. Chem. Phys.* **128**, 114714 (2008).

¹⁷P. Delaney and J. C. Greer, *Phys. Rev. Lett.* **93**, 036805 (2004).

¹⁸A. Ferretti, A. Calzolari, R. Di Felice, F. Manghi, M. J. Caldas, M. Buongiorno Nardelli, and E. Molinari, *Phys. Rev. Lett.* **94**, 116802 (2005).

¹⁹K. Thygesen, *Phys. Rev. Lett.* **100**, 166804 (2008).

²⁰P. Myöhänen, A. Stan, G. Stefanucci, and R. van Leeuwen, *Europhys. Lett.* **84**, 67001 (2008).

²¹A. Cehovin, H. Mera, J. H. Jensen, K. Stokbro, and T. B. Pedersen, *Phys. Rev. B* **77**, 195432 (2008).

²²C. Verdozzi, G. Stefanucci, and C.-O. Almbladh, *Phys. Rev. Lett.* **97**, 046603 (2006).

²³T. Frederiksen, M. Paulsson, M. Brandbyge, and A.-P. Jauho, *Phys. Rev. B* **75**, 205413 (2007).

²⁴M. Galperin, A. Nitzan, and M. A. Ratner, *Phys. Rev. B* **78**, 125320 (2008).

²⁵P. Bokes and R. W. Godby, *Phys. Rev. B* **69**, 245420 (2004).

²⁶P. Bokes, J. Jung, and R. Godby, *Phys. Rev. B* **76**, 125433 (2007).

²⁷N. Sai, M. Zwolak, G. Vignale, and M. Di Ventra, *Phys. Rev. Lett.* **94**, 186810 (2005).

²⁸J. Jung, P. Bokes, and R. W. Godby, *Phys. Rev. Lett.* **98**, 259701 (2007).

²⁹G. Onida, L. Reining, and A. Rubio, *Rev. Mod. Phys.* **74**, 601 (2002).

³⁰H. Bruus and K. Flensberg, *Many-body Quantum Theory in Condensed Matter Physics: An Introduction* (Oxford University Press, New York, 2004).

³¹P. Hohenberg and W. Kohn, *Phys. Rev.* **136**, B864 (1964).

³²W. Kohn and L. J. Sham, *Phys. Rev.* **140**, 1133 (1965).

³³X. Gonze, J.-M. Beuken, R. Caracas, F. Detraux, M. Fuchs, G.-M. Rignanese, L. Sindic, M. Verstraete, G. Zerah, F. Jollet, M. Torrent, A. Roy, M. Mikami, Ph. Ghosez, J.-Y. Raty, and D. C. Allan, *Comput. Mater. Sci.* **25**, 478 (2002).

³⁴S. Boeck, C. Freysoldt, A. Alsharif, A. Dick, L. Ismer, A. Qteish, and J. Neugebauer, <http://www.sfhingx.de>.

³⁵N. Troullier and J. L. Martins, *Phys. Rev. B* **43**, 1993 (1991).

³⁶S. G. Louie, S. Froyen, and M. L. Cohen, *Phys. Rev. B* **26**, 1738 (1982).

³⁷H. N. Rojas, R. W. Godby, and R. J. Needs, *Phys. Rev. Lett.* **74**, 1827 (1995).

³⁸A. Maeland and T. Flanagan, *Can. J. Phys.* **42**, 2364 (1964).

³⁹D. Sanchez-Portal, E. Artacho, J. Junquera, P. Ordejon, A. Garcia, and J. M. Soler, *Phys. Rev. Lett.* **83**, 3884 (1999).

⁴⁰C. Hartwigsen, S. Goedecker, and J. Hutter, *Phys. Rev. B* **58**, 3641 (1998).

⁴¹A. Marini, G. Onida, and R. Del Sole, *Phys. Rev. Lett.* **88**, 016403 (2001).

⁴²M. Shishkin and G. Kresse, *Phys. Rev. B* **74**, 035101 (2006).

⁴³P. E. Blöchl, *Phys. Rev. B* **50**, 17953 (1994).

⁴⁴P. Jelfinek, R. Pérez, J. Ortega, and F. Flores, *Phys. Rev. B* **77**, 115447 (2008).